Molecular Vision 2016; 22:1103-1121 <http://www.molvis.org/molvis/v22/1103>
Received 14 October 2015 | Accepted 21 September 2016 | Published 23 September 2016

p27^{KIP1} loss promotes proliferation and phagocytosis but prevents epithelial–mesenchymal transition in RPE cells after photoreceptor damage

Reeshan ul Quraish,[1,2] Norihiro Sudou,[1] Kaori Nomura-Komoike,[1] Fumi Sato,[2] Hiroki Fujieda[1]

[1]Department of Anatomy, School of Medicine, Tokyo Women's Medical University, Tokyo, Japan; [2]Department of Anatomy, School of Medicine, Toho University, Tokyo, Japan

Purpose: p27^{KIP1} (p27), originally identified as a cell cycle inhibitor, is now known to have multifaceted roles beyond cell cycle regulation. p27 is required for the normal histogenesis of the RPE, but the role of p27 in the mature RPE remains elusive. To define the role of p27 in the maintenance and function of the RPE, we investigated the effects of p27 deletion on the responses of the RPE after photoreceptor damage.

Methods: Photoreceptor damage was induced in wild-type (WT) and p27 knockout (KO) mice with N-methyl-N-nitrosourea (MNU) treatment. Damage-induced responses of the RPE were investigated with bromodeoxyuridine (BrdU) incorporation assays, immunofluorescence, and terminal deoxynucleotidyl transferase dUTP nick end labeling (TUNEL) assays at different stages after MNU treatment. Subcellular localization of p27 in the WT RPE was also analyzed in vivo and in vitro.

Results: MNU treatment induced photoreceptor-specific degeneration in the WT and KO retinas. BrdU incorporation assays revealed virtually no proliferation of RPE cells in the WT retinas while, in the KO retinas, approximately 16% of the RPE cells incorporated BrdU at day 2 after MNU treatment. The RPE in the KO retinas developed aberrant protrusions into the outer nuclear layer in response to photoreceptor damage and engulfed outer segment debris, as well as TUNEL-positive photoreceptor cells. Increased phosphorylation of myosin light chains and their association with rhodopsin-positive phagosomes were observed in the mutant RPE, suggesting possible deregulation of cytoskeletal dynamics. In addition, WT RPE cells exhibited evidence of the epithelial–mesenchymal transition (EMT), including morphological changes, induction of α-smooth muscle actin expression, and attenuated expression of tight junction protein ZO-1 while these changes were absent in the KO retinas. In the normal WT retinas, p27 was localized to the nuclei of RPE cells while nuclear and cytoplasmic p27 was detected in RPE cells undergoing EMT, suggesting a role for cytoplasmic p27 in the phenotype changes of RPE cells.

Conclusions: p27 loss promoted proliferation and phagocytic activity of RPE cells while preventing EMT after photoreceptor damage. These findings provide evidence for the role of p27 in the control of RPE responses to retinal damage.

Cell cycle progression is driven by cell cycle–specific cyclins assembled with their catalytic partners, cyclin-dependent kinases (CDKs). The activity of cyclin/CDK complexes is regulated by CDK inhibitors, which inhibit cell cycle progression and promote cell cycle exit [1,2]. p27^{KIP1} (p27), a member of the CIP/KIP family of CDK inhibitors, was initially considered as a tumor suppressor based on p27's ability to block cell proliferation; however, p27 is now known to have multifaceted roles beyond cell cycle regulation [3,4]. For example, p27 promotes cell migration by blocking the activation of the small GTPase RhoA [5,6], facilitates neuronal differentiation by stabilizing Neurogenin2 [5], forms a repressive complex with p130/E2F4 to regulate transcription of its target genes [7,8], and induces the epithelial–mesenchymal transition (EMT) in cancer cells via signal transducer and activator of transcription 3 (STAT3) activation [9]. Importantly, the biologic effects of p27 are regulated by its subcellular localization; cytoplasmic accumulation of p27 promotes tumor metastasis and thus is considered oncogenic [10].

Previous analyses of p27-deficient mice revealed that p27 is essential for the normal histogenesis of many organs, including the retina [11-13]. Inactivation of p27 extends the period of progenitor proliferation during retinal development and induces retinal dysplasia due to reactive gliosis of Müller glia, the principal glial cell type in the retina [14-16]. In the mature retina, p27 is predominantly expressed in Müller glia and downregulated when they reenter the cell cycle after retinal damage [16]. In addition, acute inactivation of p27 induces proliferation of Müller glia without retinal damage [17]. Thus, p27 seems to play a critical role in maintaining the quiescence of Müller glia in the mature retina.

Correspondence to: Hiroki Fujieda, Department of Anatomy, Tokyo Women's Medical University, 8-1 Kawada-cho, Shinjuku-ku, Tokyo 162-8666, Japan; Phone:+81-3-3353-8111; FAX:+81-3-5269-7405; email: hfujieda@research.twmu.ac.jp

p27 is also required for normal cell cycle exit of the RPE during development [18,19]. The RPE is a monolayer of epithelial cells located between the neural retina and the choroid and plays critical roles in the maintenance of photoreceptor function [20]. The RPE lacking p27 exhibits increased nuclear density and epithelial thickness, as well as disruption of the normal contact between the RPE and photoreceptor outer segments [19]. This implies the possibility that the absence of p27 may affect not only the development of the RPE but also its function and maintenance in the mature retina. Although the mature RPE is mitotically quiescent, it is capable of proliferation in dissociated cultures [21,22] or even in vivo under certain pathological conditions such as retinal detachment [23,24]. High-density cultures stop RPE proliferation via upregulation of p27 [25], indicating that p27 regulates proliferation of mature RPE cells at least in vitro. However, there are conflicting reports on whether the mature RPE expresses p27 [18,26], and in vivo evidence for the role of p27 in the mature RPE is lacking.

To define the role of p27 in the mature RPE in vivo, we exploited a mouse model of photoreceptor damage induced by N-methyl-N-nitrosourea (MNU) treatment [27] and analyzed the effects of the genetic deletion of p27 on the damage-induced responses of the RPE. In the absence of p27, a significantly higher proportion of RPE cells reentered the cell cycle after photoreceptor damage. In addition, we unexpectedly found that p27 loss enhanced phagocytosis of dead photoreceptors by the RPE. Moreover, EMT-like changes observed in the wild-type RPE were absent in the p27-deficient RPE. Our data provide evidence for previously unrecognized roles for p27 in the control of damage-induced RPE responses.

METHODS

Animals: $p27^{+/-}$ mice on a C57BL/6 background [13] were obtained from the Jackson Laboratory (Bar Harbor, MA) and bred and genotyped by PCR as recommended by the Jackson Laboratory. C57BL/6 mice were purchased from Charles River Laboratories Japan (Yokohama, Japan). All experimental procedures were conducted in accordance with a research protocol approved by the institutional animal care committee of Tokyo Women's Medical University and adhered to the ARVO Statement for Use of Animals in Research.

MNU treatment and tissue preparation: To induce photoreceptor damage, 5-week-old wild-type (WT) and $p27^{-/-}$ (knockout, KO) mice were treated with MNU (Sigma, St. Louis, MO, 60 mg/kg i.p.) and killed by cervical dislocation in the middle of the light phase (12 h:12 h light-dark cycle) at different time intervals after MNU treatment (at least three animals per stage and genotype). For immunohistochemistry, the eyecups were dissected and fixed with immersion in 4% paraformaldehyde. Cryostat sections were cut at 10 µm through the optic disc along the dorsoventral axis and collected on Matsunami adhesive silane (MAS)-coated glass slides (Matsunami Glass, Kishiwada, Japan). For whole mount preparations, the neural retina was separated from the RPE, choroid, and sclera following fixation. For real-time (RT)–PCR, the retinas were dissected and kept frozen at −80 °C until use.

RPE cell culture: The eyes were removed from 5-week-old WT mice after euthanasia by cervical dislocation. After digestion with 2% dispase II (Wako, Osaka, Japan) in Dulbecco's modified eagle's medium (DMEM) High Glucose (Nacalai Tesque, Kyoto, Japan) for 1 h at 37 °C, the RPE was separated, cut into small pieces with microdissection scissors, and cultured on glass bottom dishes (CELLview, Greiner Bio-One, Frickenhausen, Germany) in DMEM supplemented with 10% fetal bovine serum (GIBCO, Grand Island, NY), 1% penicillin/streptomycin (Nacalai Tesque), 2.5 mM L-glutamine (Nacalai Tesque), and 1% non-essential amino acids (Nacalai Tesque) at 37 °C in 10% CO_2 for up to 3 days. RPE cells were then fixed in 4% paraformaldehyde and processed for immunohistochemistry.

Immunofluorescence: Immunofluorescence was conducted as described previously [28]. Primary antibodies are listed in Table 1. Secondary antibodies include donkey anti-mouse immunoglobulin G (IgG; Alexa Fluor 488 and 648), donkey anti-rabbit IgG (Alexa Fluor 488 and 555), and donkey anti-rat IgG (Alexa Fluor 594), all of which were purchased from Life Technologies (Eugene, OR). Alexa Fluor 488 phalloidin (Life Technologies) was used to label actin filaments. Horseradish peroxidase (HRP)-conjugated donkey anti-rabbit IgG (Jackson Immuno Research, West Grove, PA) and the TSA Plus fluorescein system (PerkinElmer, Waltham, MA) were used for whole mount staining for Iba1. Fluorescence images were obtained using a confocal laser scanning microscope (LSM510/710; Carl Zeiss, Jena, Germany).

BrdU incorporation assay: To label S-phase cells, animals were injected with BrdU (Sigma, 100 mg/kg i.p.) 2 h before they were euthanized. For BrdU immunolabeling, the samples were treated with 2 M HCl at 37 °C for 30 min before incubation with primary antibodies.

TUNEL assay: Terminal deoxynucleotidyl transferase dUTP nick end labeling (TUNEL) assay was performed using the in situ cell death detection kit, TMR red (Roche, Mannheim, Germany) according to the manufacturer's instruction. When the TUNEL assay was combined with immunofluorescence,

the assay was first performed followed by the immunofluorescence procedure.

Image analysis: The proliferation of Müller glia and RPE cells was quantitated based on BrdU incorporation assays. Vertically sliced retinal sections containing the optic nerve head were used for analysis (three sections per animal, three animals per stage and genotype). Confocal images (at least six per animal), measuring 226 × 226 µm, were captured from the central retina, defined as 700 µm from the border of the optic nerve head, using a 40× objective lens. The number of Sox9-positive Müller glia and RPE cells, as well as BrdU-/Sox9-positive cells, was counted, and the percentages of BrdU-positive Müller glia and RPE cells were calculated. The areas of the outer nuclear layer (ONL) were measured using rhodopsin-stained retinal sections. Confocal images (at least four per animal) were obtained from the central retina as above, and the areas of the ONL measured using ImageJ software (NIH) and expressed as percentages relative to the intact WT retinas. Statistical analysis was performed with the Student *t* test, and a p value of less than 0.05 was considered statistically significant.

Quantitative RT–PCR: Retinas from both eyes of individual animals were pooled, from which total RNA was isolated using the RNeasy kit (Qiagen, Tokyo, Japan). Samples from three animals were obtained per genotype. RNA was reverse-transcribed using the ReverTra Ace qPCR RT Master Mix with gDNA Remover Kit (Toyobo, Osaka, Japan). Quantitative PCR was performed with StepOnePlus (Applied Biosystems, Tokyo, Japan) using THUNDERBIRD SYBR qPCR Mix (Toyobo). The PCR conditions consisted of an initial denaturation step (95 °C for 2 min), followed by 40 cycles of two-step PCR (95 °C for 15 s and 60 °C for 30 s). The primers were as follows: 5′-GGA GAC TGG AGC CAA CAG AG-3′ and 5′-TCT TGT CTG GCT GTG TCC TG-3′ for *Cx3cr1*; 5′-CAT TGC TGT ACA CCG TCC TG-3′ and 5′-AAC TTG GCA CAC CAA GGT TC-3′ for *P2ry12*; 5′-GAC TCA GTG AGC CCC ATC AT-3′ and 5′-AGA TCG TCT TGG CAG ATG CT-3′ for *Itgam*; and 5′-AGA ATA AGA GAG CCA CGG AC-3′ and 5′-CAA CTT CTG CAC AAC TCT AGC-3′ for *Tbp*. The relative expression of the target genes in the KO retinas compared to the WT retinas was calculated with the ΔΔCT method using *Tbp* as an internal control. Statistical analysis was performed with the Student *t* test, and a p value of less than 0.05 was considered statistically significant.

RESULTS

p27 loss induces cell cycle reentry of Müller glia and RPE cells after photoreceptor damage: To confirm the induction of photoreceptor cell death with MNU treatment, we performed TUNEL assays. In the WT and KO retinas, most photoreceptors in the ONL were TUNEL-positive by day 2 after MNU treatment while no labeling was observed in the intact retinas of both genotypes (Figure 1A).

We next conducted BrdU incorporation assays to examine the proliferative response of the WT and KO retinas after photoreceptor damage. Double immunofluorescence was performed for BrdU, an S-phase marker, and Sox9, which labels the nuclei of Müller glia, astrocytes, as well as RPE cells [29]. In the WT retinas, virtually no BrdU-positive Müller glia were detected at all stages examined after MNU treatment while a few RPE cells incorporated BrdU at day 2 and 3 (Figure 1B,C). In the KO retinas, the nuclei of many Müller glia were displaced toward the ONL even in the non-treated control retinas as reported previously [17], and some, although few (approximately 1%), Müller glia were labeled for BrdU at day 2 and 3 after MNU treatment (Figure 1B,C). A higher proportion of RPE cells (approximately 16%) were labeled for BrdU at day 2 in the mutant retinas (Figure 1B,C). Interestingly, the thickness of the RPE, as assessed with the melanosome distribution under differential interference contrast (DIC) imaging, was markedly increased in the mutant retinas by day 2 but returned to control levels by day

Table 1. List of primary antibodies.

Antibody	Dilution	Species	Source
$p27^{KIP1}$	1:1000	Mouse	BD 610241
Sox9	1:2000	Rabbit	Millipore AB5535
BrdU	1:200	Rat	Abcam ab6326
Myosin VIIa	1:2000	Rabbit	Proteus 25–6790
Rhodopsin	1:5000	Mouse	Sigma O4886
Iba1	1:2000	Rabbit	Wako 019–19741
Phospho-myosin light chain 2 (Ser19)	1:25	Rabbit	Cell Signaling 3671
α-smooth muscle actin	1:1000	Mouse	Sigma A5228
ZO-1	1:3000	Rabbit	Invitrogen 40–2200

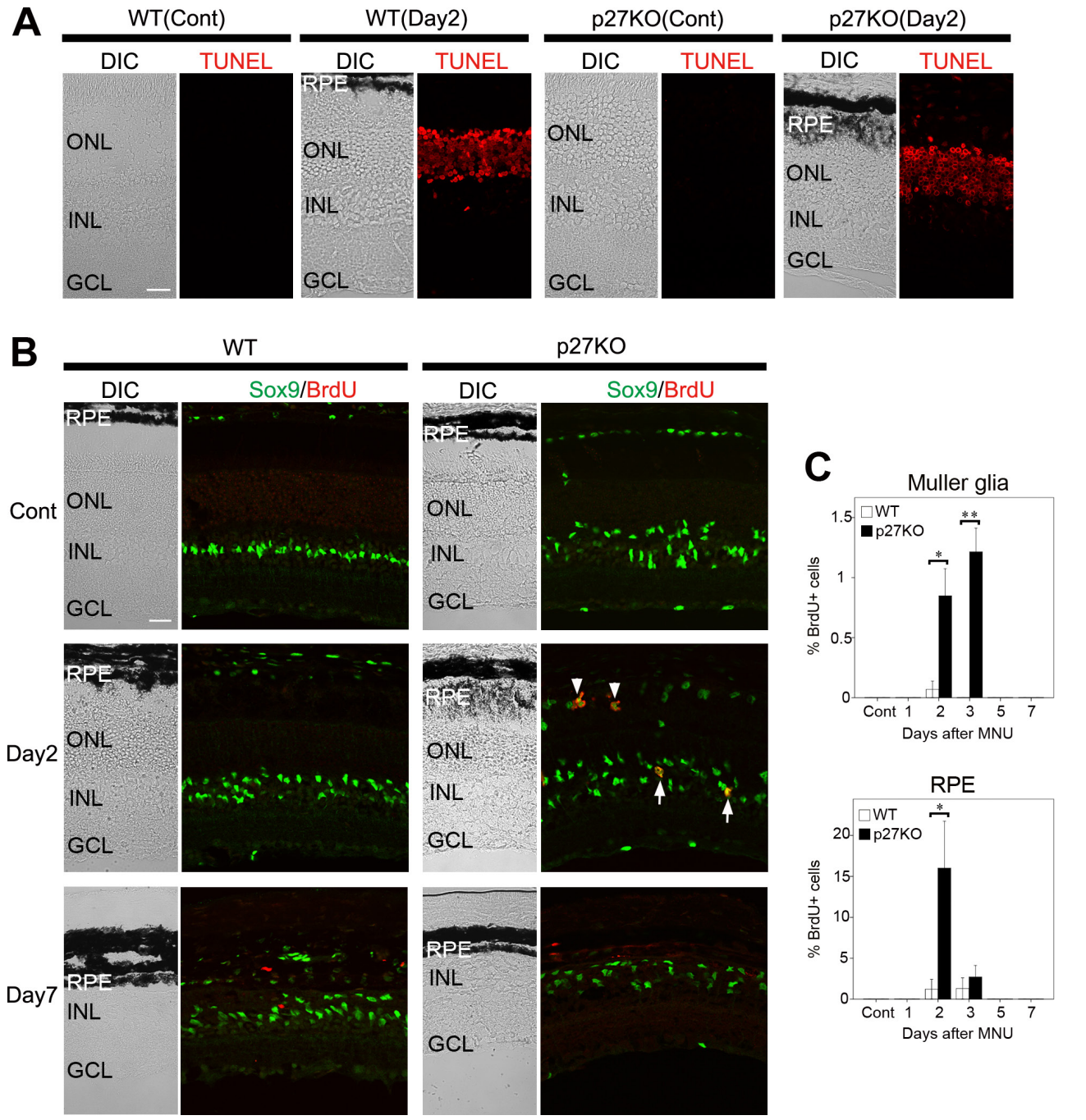

Figure 1. Proliferation of Müller glia and RPE cells in the WT and p27 KO retinas after MNU-induced photoreceptor damage. **A**: Terminal deoxynucleotidyl transferase dUTP nick end labeling (TUNEL) assays. In the wild-type (WT) and knockout (KO) retinas, most photoreceptor cells in the outer nuclear layer (ONL) are labeled at day 2 after MNU treatment while no labeling is observed in the non-treated control retinas (Cont). **B**: Double immunofluorescence for Sox9 and bromodeoxyuridine (BrdU). Note BrdU-/Sox9-positive Müller glia (arrows) and RPE cells (arrowheads) in the KO retinas at day 2. Virtually no BrdU-positive Müller glia or RPE cells are observed in the WT retinas. **C**: The proportion of BrdU-positive Müller glia and RPE cells in the central retina. Each bar represents the mean ± standard error of the mean (SEM; n = 3). Asterisks denote statistically significant differences between the WT and KO retinas (*p<0.05; **p<0.01). DIC, differential interference contrast; INL, inner nuclear layer; GCL, ganglion cell layer. Scale bars = 20 µm.

7 (Figure 1A,B). These data indicate that p27 loss induces cell cycle reentry of RPE cells in response to photoreceptor damage. The effect of p27 loss on Müller glia proliferation was less pronounced at least in the present photoreceptor damage model.

p27 loss promotes the phagocytic clearance of dead photoreceptors by the RPE: The relatively high proportion of RPE cells entering the cell cycle and the dramatic changes in the thickness of the RPE in the p27 KO retinas (Figure 1B,C) prompted us to examine the effects of p27 loss on the structure of the RPE after photoreceptor damage. We performed immunofluorescence for the RPE-specific marker myosin VIIa [30,31] to visualize the RPE cells. DIC and myosin VIIa images of the non-treated controls revealed a thin monolayer appearance of the RPE in both genotypes (Figure 2). After MNU treatment, the thickness and irregularity of the WT RPE gradually increased, and it exhibited a thick, multilayered appearance with vacuoles by day 5 although the thickness subsequently decreased by day 7 (Figure 2). The RPE of the KO retinas underwent more rapid structural changes after MNU treatment. The mutant RPE developed many folds and protrusions toward the ONL as early as day 1, when only a slight irregularity in the contour of the WT RPE was observed (Figure 2). These RPE protrusions seemed to invade the ONL by day 3 (Figure 2). Such invasion of the RPE into the ONL was never observed in the WT retina at any stage after MNU treatment. By day 5, the RPE of the mutant retinas lost abnormal protrusions and returned to the normal epithelial appearance (Figure 2).

The RPE is known for its ability to phagocytose outer segment tips shed daily by photoreceptor cells [20,32]. Previous reports have also suggested the ability of RPE cells to phagocytose photoreceptor debris after damage [27,33]. We thus hypothesized that the abnormal protrusions of the mutant RPE invading into the ONL may represent an enhanced phagocytic ability of the RPE in the absence of p27. To test this hypothesis, we first performed immunolabeling for the rod-specific marker rhodopsin to examine the time schedules of photoreceptor clearance after MNU-induced photoreceptor damage. In the non-treated controls, rhodopsin labeling was mainly localized to the photoreceptor outer segments, and there was no significant difference in the ONL thickness between the WT and KO retinas (Figure 3A,B). Rhodopsin labeling in the ONL was notably enhanced after MNU treatment (Figure 3A) possibly due to impaired rhodopsin trafficking [34]. At day 3, no significant difference in the ONL thickness was observed between genotypes; however, the rhodopsin-labeled outer segments were virtually lost in the KO retinas by day 3 while they were still present in the WT retinas (Figure 3A). Thereafter, rhodopsin-positive photoreceptors were more drastically cleared in the KO retinas compared to the WT retinas, leading to a significant difference in the ONL thickness between genotypes at day 5 (Figure 3A,B). Thus, the clearance of dead photoreceptors seemed to be accelerated in the KO retinas although most photoreceptors were eventually removed in both genotypes by day 7.

We next examined phagocytic engulfment of photoreceptor debris by the RPE using double immunofluorescence for myosin VIIa and rhodopsin. We also performed myosin VIIa immunolabeling in combination with TUNEL assays to visualize phagocytosis of dead photoreceptor nuclei by the RPE. In the control retinas of both genotypes, few rhodopsin-positive structures were visible in the RPE, and no TUNEL-positive cells were observed (Figure 3C). In the WT retinas, a few rhodopsin-positive vesicular structures, most likely phagosomes containing photoreceptor debris, were evident in the RPE by day 3, and these structures further accumulated by day 5 (Figure 3C). The engulfment of TUNEL-positive photoreceptor nuclei by the RPE was rarely observed in the WT retinas (Figure 3C). In the KO retinas, numerous rhodopsin-positive vesicles were observed in the RPE at day 3; moreover, RPE protrusions seemed to engulf the rhodopsin-positive photoreceptor cell bodies located in the ONL (Figure 3C). Myosin VIIa and TUNEL labeling also revealed engulfment of the TUNEL-positive photoreceptor nuclei by the RPE (Figure 3C). Engulfment of photoreceptor nuclei by the RPE was also confirmed with DNA labeling in whole mount RPE preparations (Figure 3D), which was never observed in the WT RPE. Rhodopsin-positive or TUNEL-positive photoreceptors were mostly eliminated in the KO retinas by day 5 (Figure 3C).

As microglia and macrophages have been considered the main players in the phagocytic clearance of dead photoreceptors [35-37], we investigated infiltration of microglia and macrophages into the ONL with double immunolabeling for rhodopsin and Iba1, a microglia- and macrophage-specific marker [38]. As expected, photoreceptor damage induced infiltration of Iba1-positive cells into the ONL in the WT and KO retinas (Figure 4A). Whole mount immunolabeling also revealed the infiltration of numerous Iba1-positive cells in the ONL by day 3 (Figure 4B). Due to their highly ramified, irregular structure, it was difficult to quantify the Iba1-positive cells accurately; however, the number of Iba1-positive cells was apparently similar between the WT and KO retinas at day 3 after MNU treatment (Figure 4B). We also analyzed the expression of microglia-specific genes (*Cx3cr1*, *P2ry12*, and *Itgam*) [39,40] with quantitative RT–PCR to compare

damage-induced microglia activation between the genotypes. At day 3 after MNU treatment, no significant difference in the expression of *Cx3cr1*, *P2ry12*, and *Itgam* was observed between genotypes (Figure 4C). Together, p27 loss does not significantly affect the infiltration and activation of microglia and macrophages after photoreceptor damage.

p27 controls cytoskeletal dynamics by inactivating RhoA, a member of the Rho family of small GTPases [3]. Because RhoA has been implicated in the control of cytoskeletal rearrangement during phagocytosis [41,42], we hypothesized that the effects of p27 loss on RPE phagocytosis may be mediated by the RhoA signaling pathway. RhoA activation induces phosphorylation of myosin light chains (MLCs), which, in turn, enhances actin–myosin interactions [43,44]. We thus investigated the distribution of phosphorylated MLC (pMLC) and its association with filamentous actin (F-actin) to test the possible deregulation of the RhoA pathway in the mutant RPE. In the control retinas of both genotypes, fluorescence-conjugated phalloidin-labeled F-actin in the apical junctions and microvilli of the RPE, as reported previously [19,45], and pMLC were colocalized with F-actin in the apical junctions (arrows in Figure 5A). pMLC labeling in the WT RPE was

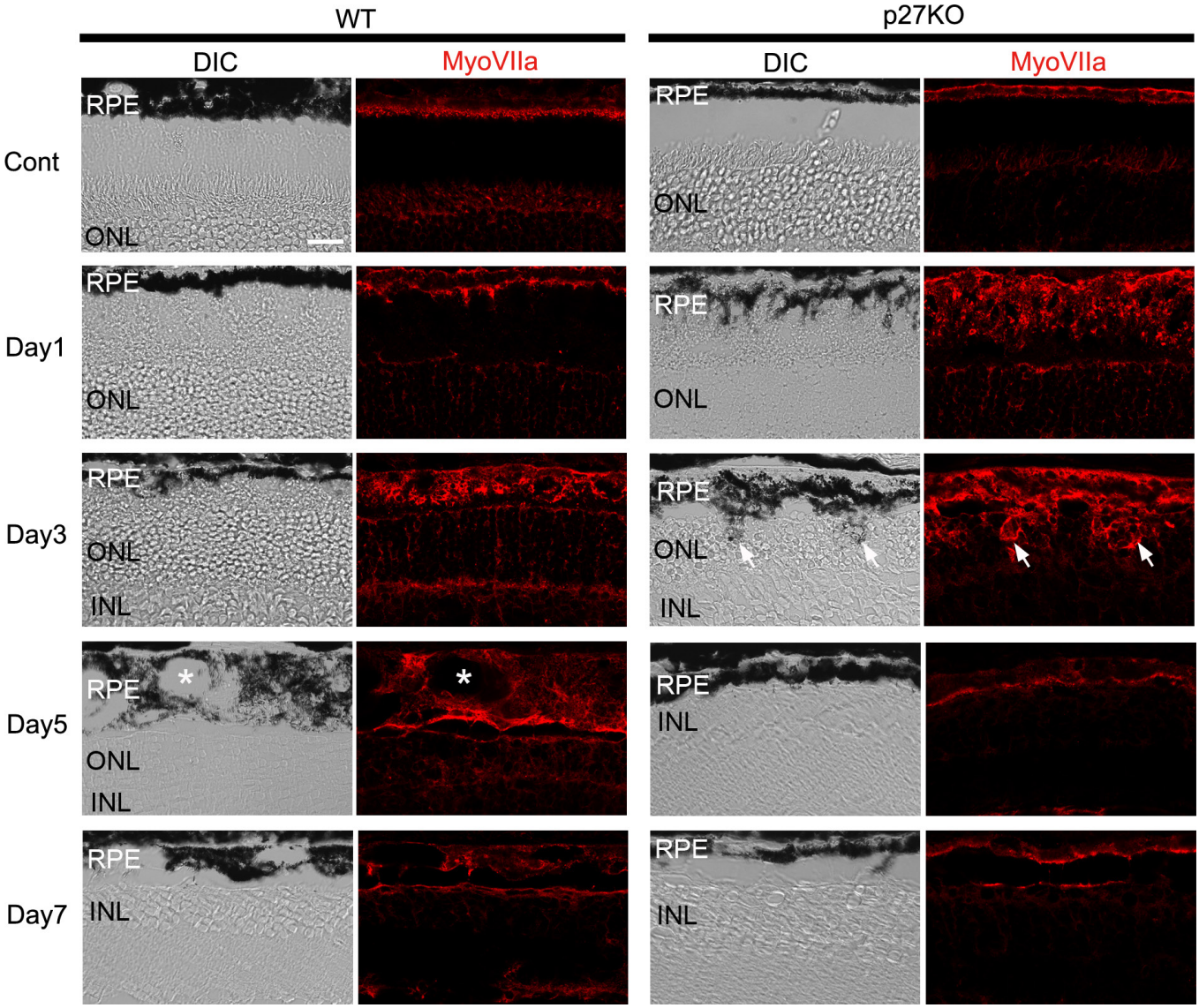

Figure 2. Myosin VIIa immunofluorescence in the RPE of the WT and p27 KO retinas after MNU treatment. The wild-type (WT) RPE becomes thicker and vacuolated (asterisks) by day 5 after MNU treatment. The RPE in the knockout (KO) retinas develops many apical protrusions as early as day 1. Arrows indicate RPE protrusions in the mutant retina invading into the outer nuclear layer (ONL) at day 3. DIC, differential interference contrast; MyoVIIa, myosin VIIa; Cont, control; INL, inner nuclear layer. Scale bar = 20 µm.

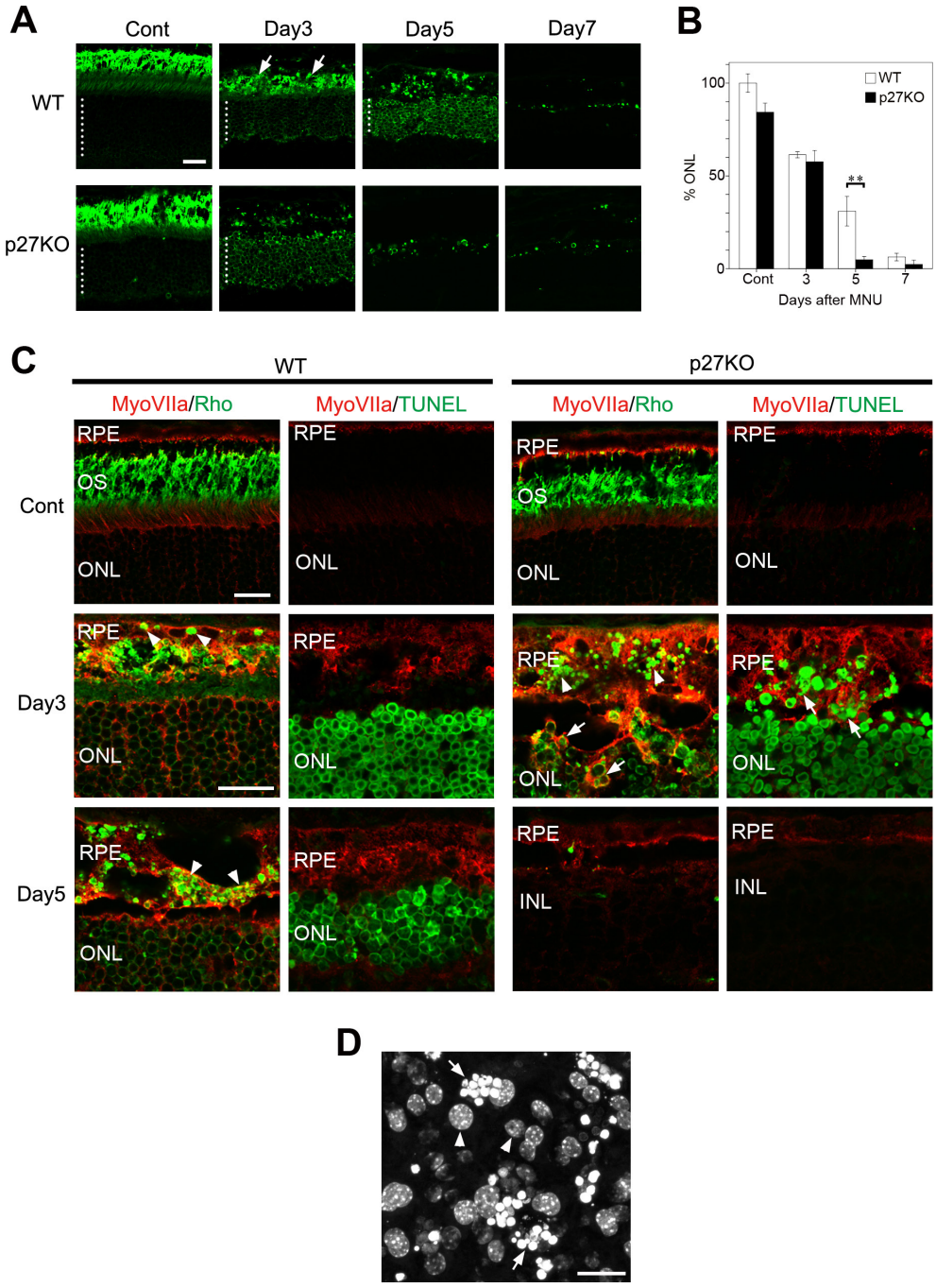

Figure 3. Enhanced phagocytosis of photoreceptor debris by the RPE in the p27 KO retinas. **A**: Rhodopsin immunofluorescence displaying the outer nuclear layer (ONL) and photoreceptor outer segments. Dotted lines indicate the thickness of the ONL. Arrows denote intensely labeled outer segment debris in the wild-type (WT) retina. Cont, control. Scale bar = 20 µm. **B**: Quantitative analysis of the areas of the ONL expressed as percentages relative to the value in the intact WT retina. Each bar represents the mean ± standard error of the mean (SEM; n = 3). Asterisks denotes statistically significant difference ($p<0.01$). **C**: Double immunofluorescence for myosin VIIa (MyoVIIa) and rhodopsin (Rho) showing an accumulation of Rho-positive phagosomes (arrowheads) in the RPE after photoreceptor damage. Engulfment of Rho-positive photoreceptor cell bodies (arrows) by the RPE is found only in the knockout (KO) retinas. Terminal deoxynucleotidyl transferase dUTP nick end labeling (TUNEL) assays combined with MyoVIIa labeling reveal dead photoreceptor nuclei (arrows) engulfed by the RPE in the KO retinas. OS, outer segments; INL, inner nuclear layer; ONL, outer nuclear layer. Scale bars = 20 µm. **D**: Nuclear staining of the whole mount RPE with Hoechst 33258 showing photoreceptor nuclei (arrows) engulfed by the mutant RPE at day 3 after N-methyl-N-nitrosourea (MNU) treatment. Arrowheads indicate the RPE nuclei.

increased only marginally in intensity after MNU treatment (Figure 5A; see day 3 and day 5 in the WT RPE) while that in the mutant RPE exhibited a dramatic increase in intensity by day 3 after MNU treatment (Figure 5A; see day 3 in the p27 KO RPE). The labeling was granular, located in the cytoplasm, and mostly colocalized with F-actin. pMLC labeling in the mutant RPE returned to normal by day 5 (Figure 5A). To test whether F-actin and/or pMLC is associated with phagosomes in the RPE, we performed triple labeling for F-actin, pMLC, and rhodopsin in the mutant retinas at day 3. As expected, F-actin and pMLC were associated with phagosomes that contained rhodopsin-positive photoreceptor debris (Figure 5B). Thus, deregulated RhoA signaling may be involved in the enhanced phagocytic activity of the RPE in the mutant retinas.

p27 loss prevents EMT in RPE cells after photoreceptor damage: The thickness of the WT RPE increased with vacuolation, and the WT RPE lost its normal monolayer structure after photoreceptor damage (Figure 2). These changes were suggestive of the EMT, known to occur in RPE cells after retinal detachment [24] or in response to metabolic or oxidative stress [46]. In our model, these EMT-like changes were maximally observed at day 5 and still apparent at day 7 in the WT RPE (Figure 2). In contrast, the RPE in the p27 KO retinas exhibited abnormal morphological changes (such as apical protrusions) at early stages (days 1–3), and the normal epithelial appearance returned by day 5 (Figure 2). Thus, we tested the possibility that p27 loss affects the EMT process in RPE cells after photoreceptor damage. To this end, we performed immunofluorescence for myosin VIIa in combination with α-smooth muscle actin (α-SMA), one of the established markers for EMT in RPE cells [22,24,47].

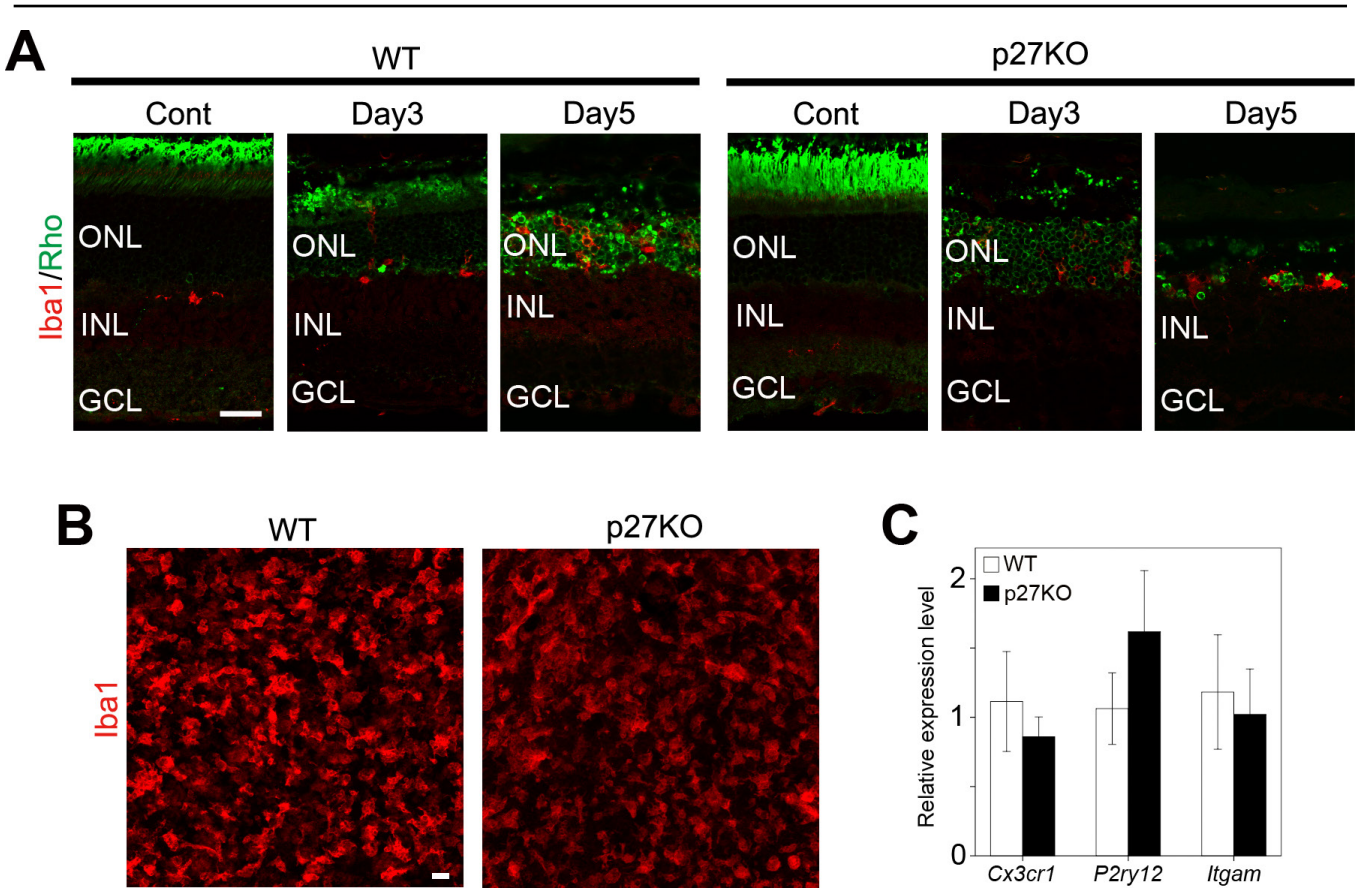

Figure 4. Infiltration of microglia and macrophages in the WT and p27 KO retinas after MNU treatment. **A**: Double immunofluorescence for Iba1 and rhodopsin (Rho) reveals infiltration of microglia and macrophages into the outer nuclear layer (ONL) after photoreceptor damage. INL, inner nuclear layer; GCL, ganglion cell layer. Scale bar = 20 µm. **B**: Z-stack images of Iba1 staining in the whole mount retinas at day 3 after N-methyl-N-nitrosourea (MNU) treatment showing infiltration of microglia and macrophages in the ONL. Scale bar = 20 µm. **C**: Quantitative real-time (RT)–PCR analysis of microglia-specific genes in the wild-type (WT) and knockout (KO) retinas at day 3 after MNU treatment. The transcript levels of each gene are expressed relative to the WT retinas after normalization to *Tbp* levels. Each bar represents the mean ± standard error of the mean (SEM; n = 3). No significant difference was observed between the WT and KO retinas.

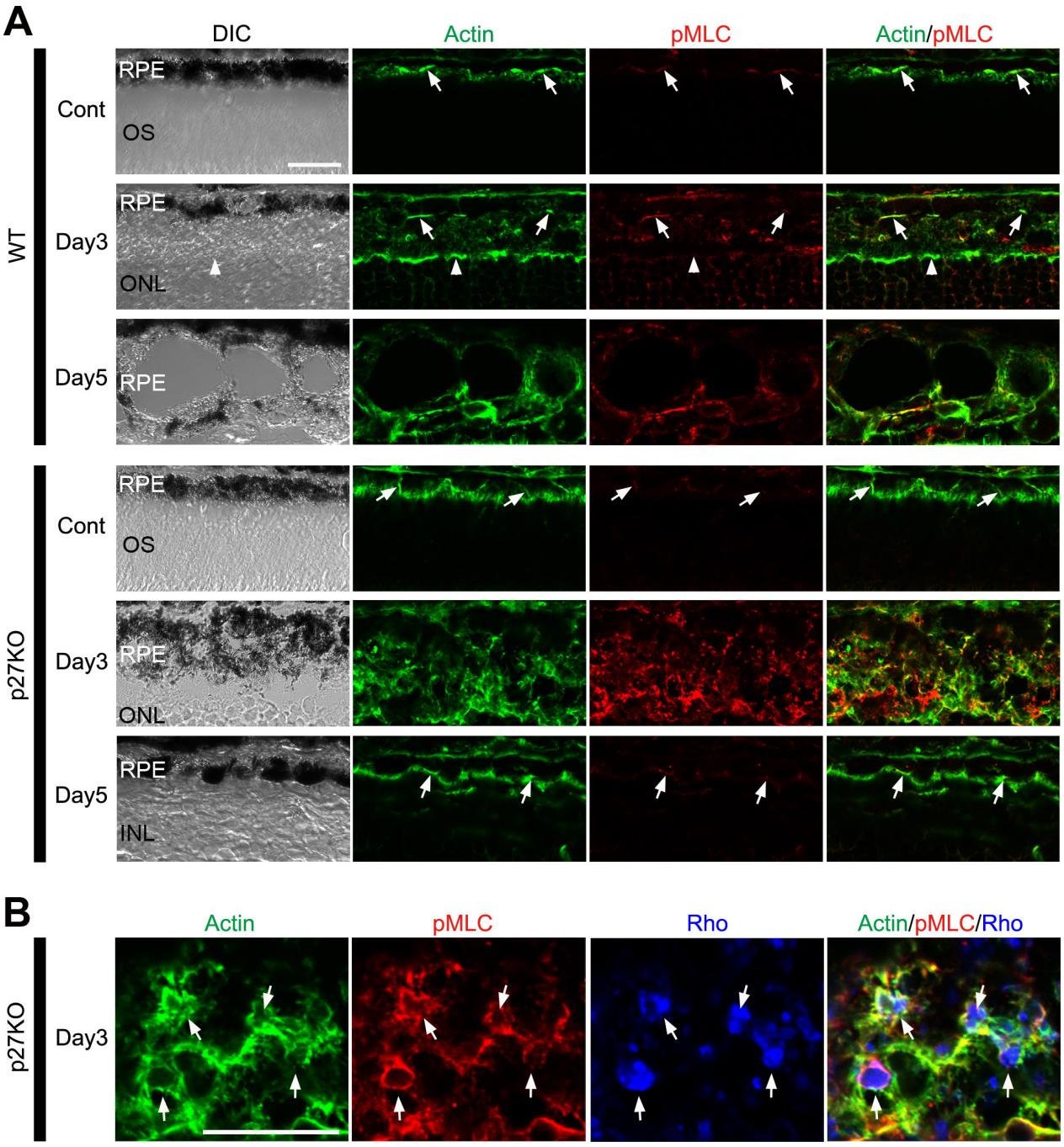

Figure 5. Enhanced phosphorylation of myosin light chains in the RPE of the p27 KO retinas after photoreceptor damage. **A**: Immunofluorescence for phosphorylated myosin light chains (pMLC) combined with phalloidin labeling. Arrows indicate colocalization of phalloidin-labeled F-actin and pMLC in the apical junctions of the RPE. The outer limiting membrane is also labeled for F-actin (arrowheads). Note enhanced labeling for F-actin and pMLC in the mutant RPE at day 3. **B**: Triple labeling for F-actin, pMLC, and rhodopsin (Rho) in the mutant RPE at day 3. Note colocalization of F-actin and pMLC with Rho-positive phagosomes (arrows). DIC, differential interference contrast; Cont, control; OS, outer segments; ONL, outer nuclear layer; INL, inner nuclear layer. Scale bars = 20 µm.

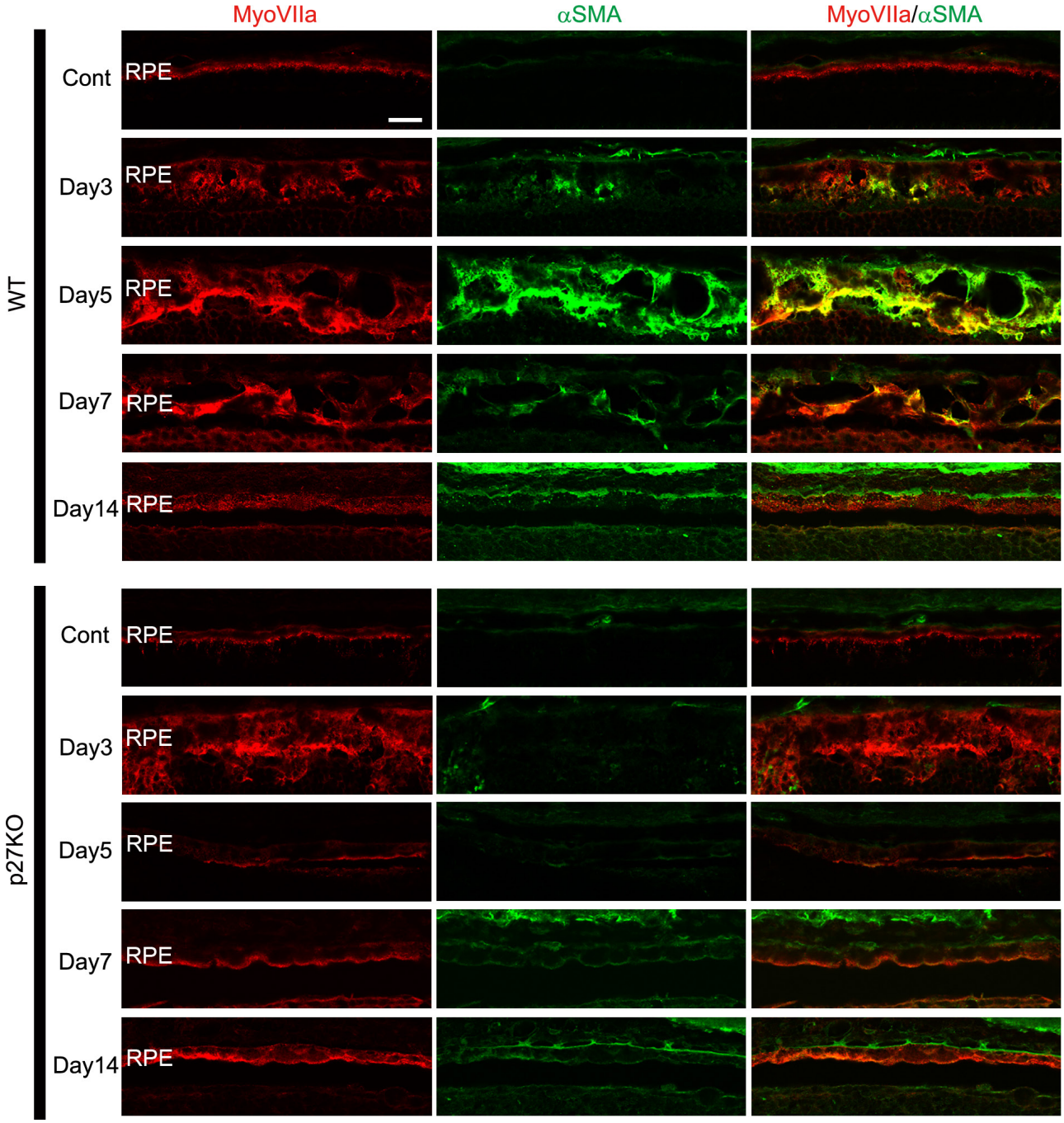

Figure 6. Expression of α-SMA in the RPE of the WT and p27 KO retinas after photoreceptor damage. α-smooth muscle actin (α-SMA) immunolabeling is transiently increased in the RPE of the wild-type (WT) retinas with the peak around day 5 after N-methyl-N-nitrosourea (MNU) treatment. Note the absence of α-SMA labeling in the mutant retinas. MyoVIIa, myosin VIIa; Cont, control. Scale bar = 20 µm.

No α-SMA labeling was detected in the control RPE of the WT and KO retinas (Figure 6). At day 3, some RPE cells in the WT retinas were faintly labeled for α-SMA, and at day 5, most RPE cells exhibiting EMT-like morphological changes were intensely labeled for α-SMA (Figure 6). α-SMA labeling in the WT RPE was subsequently decreased and virtually lost by day 14, when the RPE reacquired its normal epithelial appearance (Figure 6). In the p27 KO retinas, in contrast, no α-SMA labeling was detected in the RPE at any stages examined after MNU treatment (Figure 6).

We next examined the expression of the tight junction protein ZO-1, known to be repressed during EMT [46,48]. In the control retinas of both genotypes, ZO-1 immunolabeling was detected in the apical junctions of the RPE and the outer limiting membrane (OLM) of the neural retina (Figure 7A), as reported previously [49]. ZO-1 labeling in the WT RPE was diminished after MNU treatment, and only faint, punctate labeling was observed at day 5, suggesting disassembly of the junctional complexes during EMT (Figure 7A). However, ZO-1 immunolabeling in the mutant RPE seemed somewhat increased after MNU treatment (Figure 7A). The labeling became irregular in appearance by day 3, likely reflecting structural alterations of the RPE, but it returned to the normal arrangement by day 5 (Figure 7A). ZO-1 labeling in the OLM was disrupted at sites where aberrant RPE protrusions invaded into the ONL (Figure 7A, asterisk). ZO-1 immunolabeling using whole mount RPE preparations revealed the morphology of individual RPE cells more clearly. The RPE cells in the intact WT retinas were polygonal in shape and uniform in size while some irregularity in the size and shape of RPE cells was observed by day 3 after MNU treatment (Figure 7B). RPE cells in the intact KO retinas were smaller and more densely packed compared to the WT retinas (Figure 7B) as reported previously [19]. The size and shape of the RPE cells in the KO retinas became considerably irregular by day 3 after MNU treatment consistent with the appearance of ZO-1 labeling on sections (Figure 7B). Taken together, α-SMA and ZO-1 expression, as well as morphological alterations, was consistent with the possibility that the lack of p27 prevents EMT in RPE cells after photoreceptor damage.

Cytoplasmic expression of p27 in RPE cells undergoing EMT: These findings indicate that p27 expression is required for the EMT process in RPE cells after photoreceptor damage. A recent report suggested that cytoplasmic p27 promotes EMT in cancer cells through upregulation of the EMT-inducing transcription factor Twist1 [9]. We thus hypothesized that cytoplasmic expression of p27 may be involved in EMT in RPE cells. To test this hypothesis, we examined the subcellular localization of p27 in RPE cells with double immunofluorescence for p27 in combination with Sox9 (which marks the nuclei of RPE cells) or myosin VIIa (which labels the RPE cell cytoplasm). p27 was detected in all nuclear layers of the control WT retinas while the staining was absent in the KO retinas, which verified antibody specificity (Figure 8A). p27 was also localized to the RPE nuclei, which colabeled with Sox9, while the mutant RPE was devoid of p27 labeling (Figure 8B). In contrast, in the WT RPE undergoing EMT (at day 5 after MNU treatment), p27 was colocalized not only with Sox9 (Figure 8C) but also with myosin VIIa (Figure 8D), indicating nuclear and cytoplasmic expression of p27 in RPE cells undergoing EMT.

We further analyzed p27 expression in primary cultures of the RPE, which are known to undergo EMT [22,47]. At day 1 in culture, α-SMA was detected in restricted regions of the RPE sheets (Figure 9A), and ZO-1 labeling was partially disorganized (Figure 9B). p27 was detected not only in the nucleus but also in the cytoplasm of the RPE cells (Figure 9B). At day 3 in culture, the RPE cells were significantly enlarged and exhibited intense α-SMA immunoreactivity throughout the cytoplasm (Figure 9A). These RPE cells with an enlarged cell body were devoid of p27 labeling in the nucleus and the cytoplasm (Figure 9B).

DISCUSSION

The present study analyzed the effects of p27 loss on the responses of the RPE to MNU-induced photoreceptor damage. Our data revealed that in addition to facilitating cell cycle reentry, p27 loss affected the phagocytic ability, as well as EMT-like phenotype changes in the RPE cells, providing the first evidence that p27 may play multifaceted roles in the regulation of damage-induced RPE responses in vivo.

MNU treatment induced photoreceptor-specific cell death in a similar manner between the WT and p27 KO retinas. Nevertheless, photoreceptor damage caused virtually no proliferation of the RPE in the WT retinas while a substantial fraction of RPE cells reentered the cell cycle in the absence of p27. This suggests that p27 plays a critical role in maintaining quiescence of the mature RPE. Our data also revealed increased cell cycle reentry of Müller glia after photoreceptor damage in the p27 KO retinas, consistent with a previous report that acute inactivation of p27 induced cell cycle reentry of this cell type [17]. However, the proportion of Müller glia reentering the cell cycle was low (approximately 1% in the central retina), indicating that p27 is dispensable in most Müller glia for maintaining quiescence in our model.

We unexpectedly found that p27 loss enhanced the phagocytic activity of the RPE in response to photoreceptor damage. The RPE is known to phagocytose outer segment

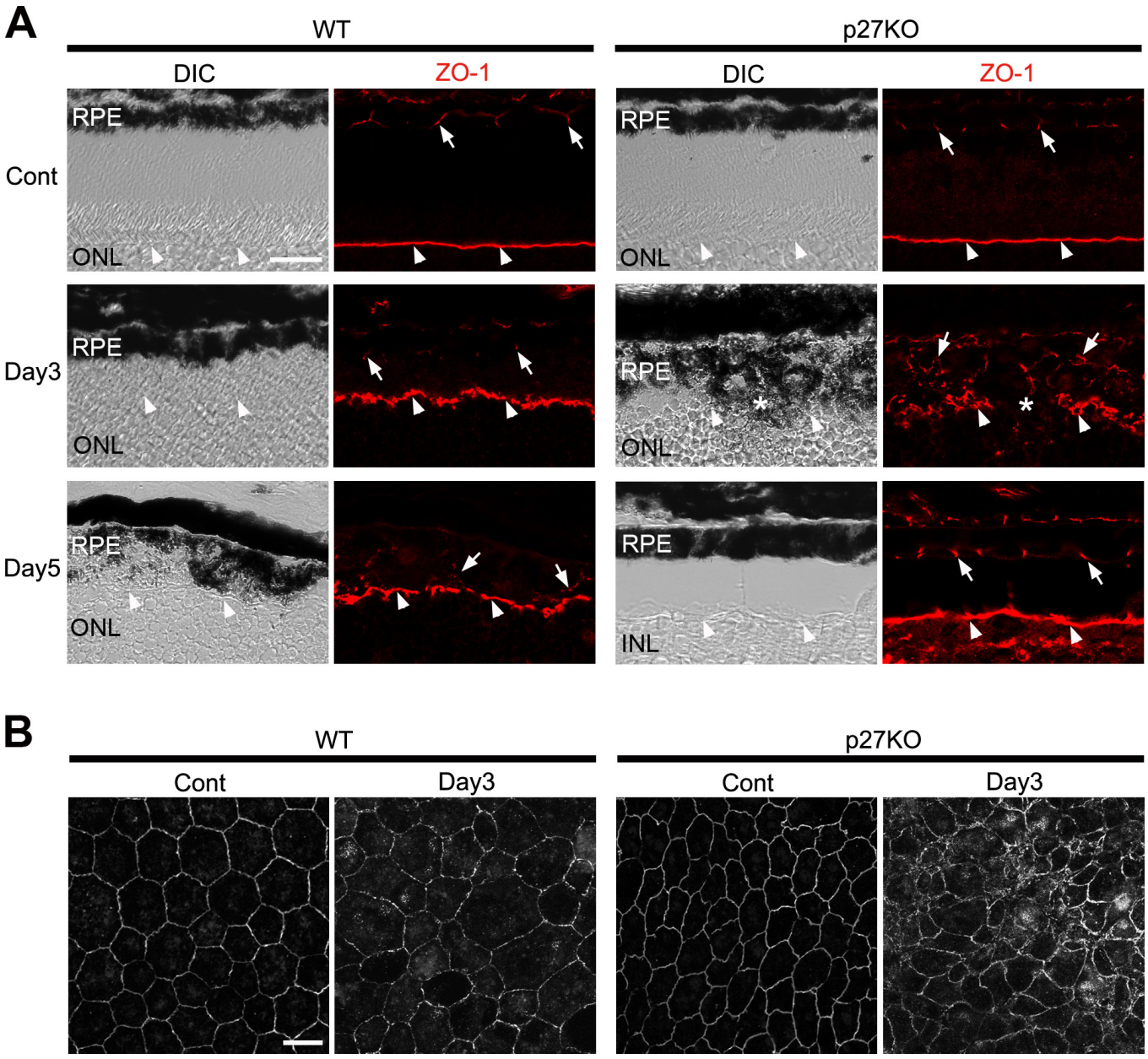

Figure 7. ZO-1 expression in the RPE of the WT and p27 KO retinas after photoreceptor damage. **A**: ZO-1 immunolabeling is detected in the apical junctions of the RPE (arrows) and the outer limiting membrane (OLM, arrowheads). In the knockout (KO) retinas, the ZO-1-labeled OLM is disrupted where the RPE protrusions invade into the ONL (asterisks). Note attenuated ZO-1 labeling in the wild-type (WT) RPE after photoreceptor damage. DIC, differential interference contrast; Cont, control; ONL, outer nuclear layer. Scale bar = 20 µm. **B**: ZO-1 immunolabeling in whole mount RPE preparations, showing the significantly irregular size and shape of mutant RPE cells at day 3 after N-methyl-N-nitrosourea (MNU) treatment. Scale bar = 20 µm.

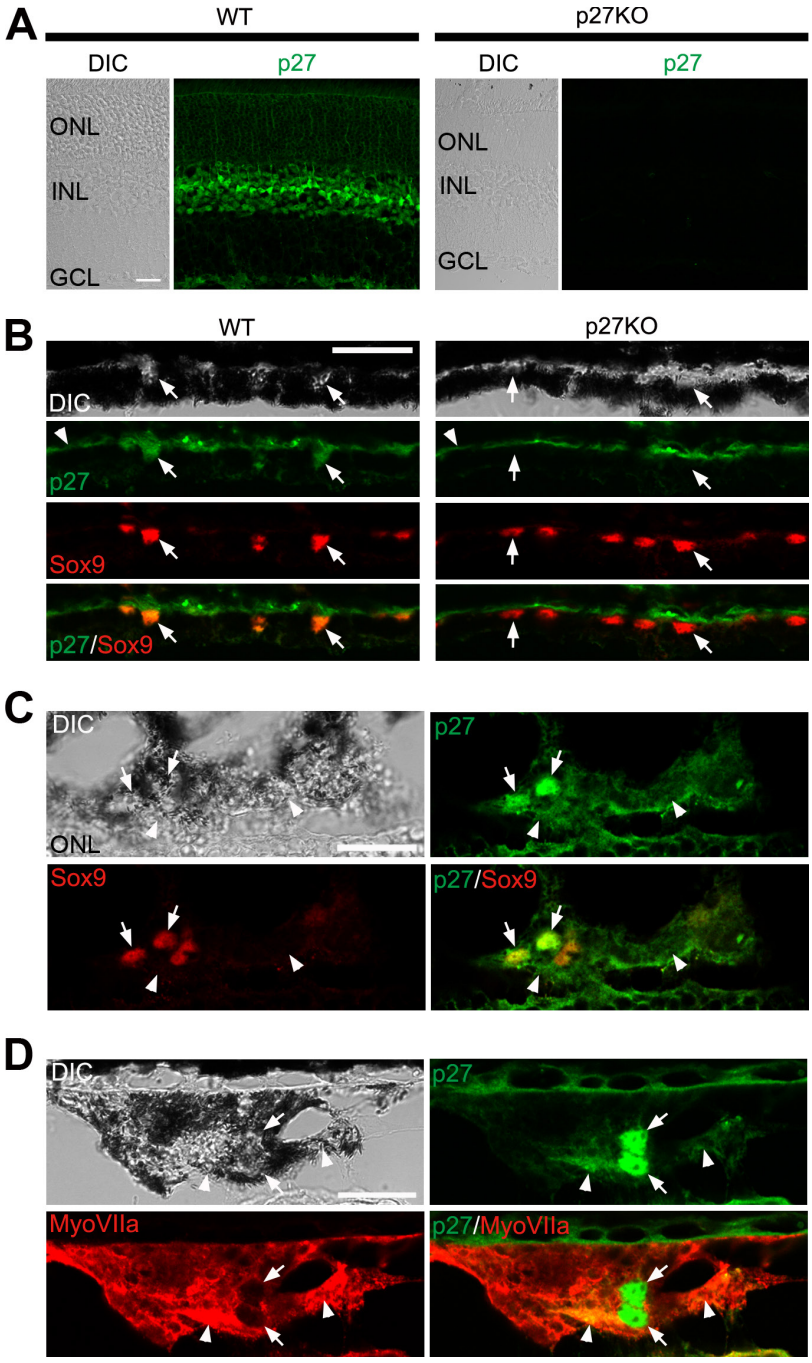

Figure 8. Subcellular localization of p27 in the RPE. **A**: Immunofluorescence for p27 in the wild-type (WT) and p27 knockout (KO) retinas. Note p27 labeling in the outer nuclear layer (ONL), inner nuclear layer (INL), and ganglion cell layer (GCL) in the WT retina and the absence of staining in the knockout (KO) retina. **B**: Double immunofluorescence for p27 and Sox9 in the RPE of the WT and p27 KO retinas. Arrows indicate the Sox9-positive RPE nuclei. Note the nuclear expression of p27 in the WT RPE and the absence of p27 in the mutant. Arrowheads denote Bruch's membrane labeled non-specifically. **C**: Double immunofluorescence for p27 and Sox9 in the WT RPE at day 5 after N-methyl-N-nitrosourea (MNU) treatment. p27 is localized not only in the nuclei (arrows) but also in the cytoplasm (arrowheads). **D**: Double immunofluorescence for p27 and myosin VIIa (MyoVIIa) in the WT RPE at day 5 after MNU treatment. Note nuclear (arrows) and cytoplasmic (arrowheads) staining for p27. DIC, differential interference contrast. Scale bars = 20 µm.

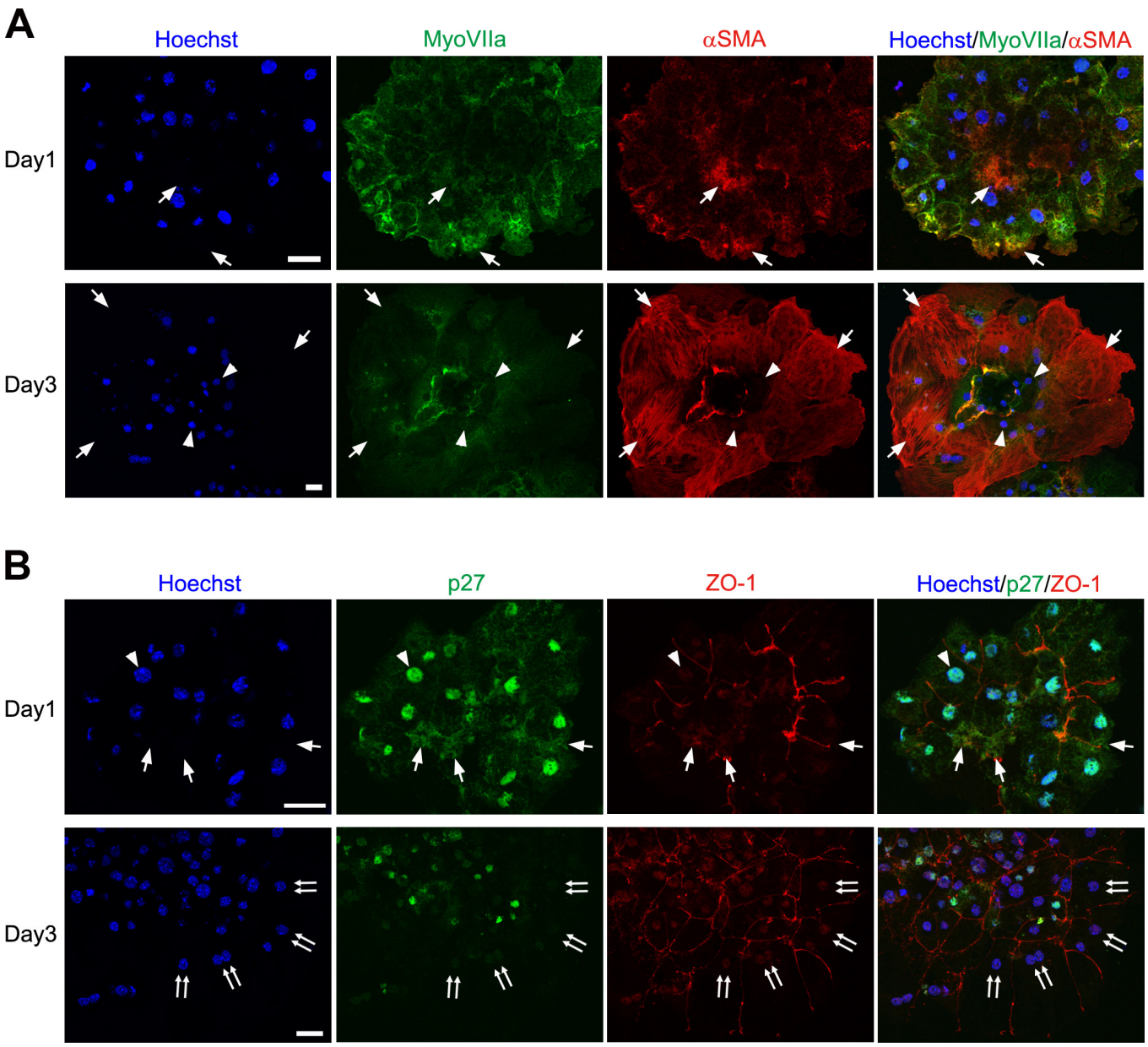

Figure 9. p27 expression in primary cultures of RPE cells. **A**: Double immunofluorescence for myosin VIIa (MyoVIIa) and α-smooth muscle actin (α-SMA) showing the epithelial–mesenchymal transition (EMT) of RPE cells in culture. Arrows indicate α-SMA-positive RPE cells while arrowheads denote α-SMA-negative RPE cells. **B**: Double immunofluorescence for p27 and ZO-1. p27 is detected in the nucleus (arrowhead) and the cytoplasm (arrows) at day 1 while nuclear and cytoplasmic p27 is lost in many RPE cells by day 3 (double arrows). Hoechst, nuclear staining with Hoechst 33258. Scale bars = 20 µm.

tips shed daily by photoreceptor cells [20,32]. Phagocytosed outer segments were also observed in the RPE after light or chemically-induced photoreceptor degeneration, suggesting that the RPE is able to remove not only the shed outer segments of intact photoreceptors but also the outer segment debris of degenerated photoreceptors [27,50]. The molecular mechanisms by which the RPE phagocytoses shed outer segments are highly similar to those used by professional phagocytes, such as macrophages for apoptotic cell clearance [51,52]. However, to our knowledge, phagocytosis of apoptotic cell bodies by the RPE has not been reported, and phagocytic targets of the RPE seem to be restricted to the photoreceptor outer segments even in pathological conditions. We observed rhodopsin-positive phagosome-like structures, most likely containing outer segment debris, in the WT RPE after photoreceptor damage, but we rarely observed TUNEL-positive

photoreceptor nuclei engulfed by the WT RPE. p27 loss does not seem to affect the normal phagocytic clearance of shed outer segments [19]; however, the p27-deficient RPE exhibited drastic responses to photoreceptor damage by extending aberrant apical protrusions and engulfing not only outer segment debris but also dead photoreceptor nuclei. The enhanced phagocytic activity of the RPE likely accelerated the removal of the ONL in the absence of p27. Alternatively, as previous reports indicated that dead photoreceptors are phagocytosed by resident microglia or monocyte-derived macrophages [35-37], it is also likely that p27 loss promoted the infiltration and phagocytic activity of microglia and macrophages. However, the infiltration of microglia and macrophages into the ONL was similar between the WT and KO retinas, and the expression of the microglia-specific genes *Cx3cr1*, *P2ry12*, and *Itgam*, known regulators of microglial activation [53-55], did not differ significantly between genotypes. Thus, we do not favor the possibility that the effects of p27 loss on microglial activation contributed significantly to accelerate the removal of dead photoreceptors.

The mechanism underlying the enhanced phagocytosis by the RPE in the absence of p27 remains elusive. Given the previous reports that phagocytosis by macrophages is regulated by the Rho GTPase-mediated cytoskeletal dynamics [41,42] and that p27 regulates cytoskeletal dynamics by preventing RhoA activation [3], we hypothesized that cytoskeletal rearrangement induced by deregulated RhoA activity may be involved in the aberrant activation of phagocytosis by the p27-deficient RPE. It has been reported that GTP-bound active RhoA increases the kinase activity of Rho-associated kinase (ROCK), a major downstream effector of RhoA, which phosphorylates MLCs and promotes actin–myosin interactions [43]. The present study revealed a large increase in MLC phosphorylation in association with the enhanced RPE phagocytosis in the absence of p27. Moreover, phosphorylated MLC and F-actin, normally associated with apical junctions, were recruited to rhodopsin-containing phagosomes, strongly indicating the involvement of the activated actomyosin complex in the process of phagosome formation. This is consistent with a previous report that the Mertk-dependent recruitment of non-muscle myosin II to phagosomes is essential for the normal phagocytosis of outer segments by RPE cells [56]. Altogether, we favor the possibility that cytoskeletal rearrangement, most likely induced by aberrant activation of the RhoA/ROCK signaling pathway, is involved in the activation of RPE phagocytosis in the absence of p27. Alternatively, given the previous reports suggesting the role of p27 as a transcriptional regulator [7,8], it would be interesting to test whether p27 loss affects the expression of phagocytic proteins in the RPE. In addition, we do not rule out the possibility that the effects of p27 loss on the RPE phagocytosis may be non-cell autonomous, for example, secondary to changes in the neural retina. Future work using RPE-specific p27 KO mice would be useful to define cell-autonomous functions of p27 in the RPE.

Another unexpected effect of p27 loss was a lack of EMT-like changes in the RPE after photoreceptor damage. EMT is a process by which epithelial cells lose their epithelial characteristics, including cell–cell junctions and apical–basal polarity, while acquiring mesenchymal phenotype, such as the ability to migrate and express mesenchymal proteins [48,57]. The RPE is known to undergo EMT in dissociated cultures [22,47], after retinal detachment [24], or in response to metabolic or oxidative stress [46]. In the present photoreceptor damage model, the WT RPE exhibited hallmarks of EMT, including disorganization of the epithelial structure, upregulation of α-SMA, and attenuation of ZO-1 expression, consistent with the previous reports of RPE cells undergoing EMT [22,24,46,47]. In contrast, these EMT-like changes were never observed in the RPE cells in the p27 KO retinas, indicating that p27 is required for the initiation of EMT in RPE cells. How p27 regulates the EMT process in RPE cells remains to be investigated. Zhao et al. recently reported that cytoplasmic p27 promotes EMT in cancer cells by activating the Janus kinase (JAK)/STAT pathway, which, in turn, induces Twist1 upregulation [9]. It would be interesting to determine whether the same mechanism regulates EMT in RPE cells. We found cytoplasmic localization of p27 in RPE cells undergoing EMT in vivo and in vitro but not in those with the normal epithelial phenotype, consistent with the role of cytoplasmic p27 in EMT. Notably, nuclear and cytoplasmic p27 was lost in RPE cells in culture that displayed an advanced EMT phenotype, such as the enlarged cell body and high α-SMA expression. Loss of p27 in the nucleus indicates that these cells are most likely proliferating. Thus, p27 may be required for the induction but not for the maintenance of EMT in RPE cells. p27, when located in the nucleus, behaves as a cell cycle inhibitor by interfering with cyclin and CDK complexes [1,3]. However, p27 also regulates cytoskeletal dynamics and cell motility when expressed in the cytoplasm [3]. Cytoplasmic accumulation of p27 is promoted by the phosphoinositide 3-kinase/protein kinase B mechanistic target of rapamycin (PI3K/AKT/mTOR) pathway via the phosphorylation of p27 at threonine 157 (T157) or T198 [3,10,58]. Intriguingly, the PI3K/AKT/mTOR pathway has been shown to drive EMT in different cell types, including the RPE [46,59-61]. It is thus tempting to speculate that this signaling pathway may control the EMT progression in RPE cells, at least, in part, through phosphorylation and cytoplasmic sequestration of p27, as has been proposed for EMT in cancer cells [9].

The present evidence for the role of p27 as a regulator of proliferation, phagocytosis, and EMT suggests the possibility that p27 may coordinate these stress-induced RPE responses under pathological conditions. EMT is commonly accompanied by proliferation in RPE cells [24,46,47,62]. However, in the present photoreceptor damage model, no proliferation of RPE cells was observed during the EMT-like changes in the WT retina. As RPE cells undergoing EMT expressed p27 in the nucleus and cytoplasm, it is likely that persistent expression of p27 in the nucleus prevented cell cycle reentry while cytoplasmic p27 acted as an EMT inducer. p27 may also link EMT with phagocytosis. Our data support the notion that p27 inhibits phagocytosis while promoting EMT, which is consistent with previous reports that the phagocytic ability of RPE cells is impaired during EMT progression [46,47,63]. The ability to phagocytose photoreceptor outer segments may be one of the epithelial characteristics of RPE cells, and thus, its inhibition may simply reflect the dedifferentiation process during EMT. Alternatively, inhibition of phagocytosis after retinal damage may have some advantage to the RPE. EMT has been known to suppress apoptosis, thus conferring a survival advantage to cells undergoing EMT [64]. Although prompt removal of degenerated cells by phagocytosis is essential for the maintenance of tissue structure and function [65,66], excessive phagocytosis by the RPE may lead to the accumulation of degradation products that induce oxidative damage to the RPE [20,32,67]. Thus, tight control of its phagocytic ability may be crucial for the preservation of RPE health, especially when the RPE is challenged by massive photoreceptor death. The present evidence that p27 controls multiple responses of the RPE after photoreceptor damage provides critical insight into the mechanisms that ensure structural and functional integrity of the RPE under pathological conditions.

ACKNOWLEDGMENTS

This work was partly supported by Grant-in-Aid for Scientific Research, No. 22591968 (to H. F.) from Japan Society for the Promotion of Science.

REFERENCES

1. Sherr CJ, Roberts JM. CDK inhibitors: positive and negative regulators of G1-phase progression. Genes Dev 1999; 13:1501-12. [PMID: 10385618].
2. Vidal A, Koff A. Cell-cycle inhibitors: three families united by a common cause. Gene 2000; 247:1-15. [PMID: 10773440].
3. Besson A, Dowdy SF, Roberts JM. CDK inhibitors: cell cycle regulators and beyond. Dev Cell 2008; 14:159-69. [PMID: 18267085].
4. Lim S, Kaldis P. Cdks, cyclins and CKIs: roles beyond cell cycle regulation. Development 2013; 140:3079-93. [PMID: 23861057].
5. Nguyen L, Besson A, Heng JI, Schuurmans C, Teboul L, Parras C, Philpott A, Roberts JM, Guillemot F. p27kip1 independently promotes neuronal differentiation and migration in the cerebral cortex. Genes Dev 2006; 20:1511-24. [PMID: 16705040].
6. Kawauchi T, Chihama K, Nabeshima Y, Hoshino M. Cdk5 phosphorylates and stabilizes p27kip1 contributing to actin organization and cortical neuronal migration. Nat Cell Biol 2006; 8:17-26. [PMID: 16341208].
7. Pippa R, Espinosa L, Gundem G, Garcia-Escudero R, Dominguez A, Orlando S, Gallastegui E, Saiz C, Besson A, Pujol MJ, Lopez-Bigas N, Paramio JM, Bigas A, Bachs O. p27Kip1 represses transcription by direct interaction with p130/E2F4 at the promoters of target genes. Oncogene 2012; 31:4207-20. [PMID: 22179826].
8. Li H, Collado M, Villasante A, Matheu A, Lynch CJ, Canamero M, Rizzoti K, Carneiro C, Martinez G, Vidal A, Lovell-Badge R, Serrano M. p27(Kip1) directly represses Sox2 during embryonic stem cell differentiation. Cell Stem Cell 2012; 11:845-52. [PMID: 23217425].
9. Zhao D, Besser AH, Wander SA, Sun J, Zhou W, Wang B, Ince T, Durante MA, Guo W, Mills G, Theodorescu D, Slingerland J. Cytoplasmic p27 promotes epithelial-mesenchymal transition and tumor metastasis via STAT3-mediated Twist1 upregulation. Oncogene 2015; 34:5447-59. [PMID: 25684140].
10. Larrea MD, Wander SA, Slingerland JM. p27 as Jekyll and Hyde: regulation of cell cycle and cell motility. Cell Cycle 2009; 8:3455-61. [PMID: 19829074].
11. Nakayama K, Ishida N, Shirane M, Inomata A, Inoue T, Shishido N, Horii I, Loh DY. Mice lacking p27(Kip1) display increased body size, multiple organ hyperplasia, retinal dysplasia, and pituitary tumors. Cell 1996; 85:707-20. [PMID: 8646779].
12. Kiyokawa H, Kineman RD, Manova-Todorova KO, Soares VC, Hoffman ES, Ono M, Khanam D, Hayday AC, Frohman LA, Koff A. Enhanced growth of mice lacking the cyclin-dependent kinase inhibitor function of p27(Kip1). Cell 1996; 85:721-32. [PMID: 8646780].
13. Fero ML, Rivkin M, Tasch M, Porter P, Carow CE, Firpo E, Polyak K, Tsai LH, Broudy V, Perlmutter RM, Kaushansky K, Roberts JM. A syndrome of multiorgan hyperplasia with features of gigantism, tumorigenesis, and female sterility in p27(Kip1)-deficient mice. Cell 1996; 85:733-44. [PMID: 8646781].
14. Dyer MA, Cepko CL. p27Kip1 and p57Kip2 regulate proliferation in distinct retinal progenitor cell populations. J Neurosci 2001; 21:4259-71. [PMID: 11404411].
15. Levine EM, Close J, Fero M, Ostrovsky A, Reh TA. p27(Kip1) regulates cell cycle withdrawal of late multipotent progenitor cells in the mammalian retina. Dev Biol 2000; 219:299-314. [PMID: 10694424].

16. Dyer MA, Cepko CL. Control of Muller glial cell proliferation and activation following retinal injury. Nat Neurosci 2000; 3:873-80. [PMID: 10966617].

17. Vazquez-Chona FR, Swan A, Ferrell WD, Jiang L, Baehr W, Chien WM, Fero M, Marc RE, Levine EM. Proliferative reactive gliosis is compatible with glial metabolic support and neuronal function. BMC Neurosci 2011; 12:98-[PMID: 21985191].

18. Yoshida K, Nakayama K, Kase S, Nagahama H, Harada T, Ikeda H, Harada C, Imaki J, Ohgami K, Shiratori K, Ohno S, Nishi S, Nakayama KI. Involvement of p27(KIP1) in proliferation of the retinal pigment epithelium and ciliary body. Anat Embryol (Berl) 2004; 208:145-50. [PMID: 15007644].

19. Defoe DM, Adams LB, Sun J, Wisecarver SN, Levine EM. Defects in retinal pigment epithelium cell proliferation and retinal attachment in mutant mice with p27(Kip1) gene ablation. Mol Vis 2007; 13:273-86. [PMID: 17356514].

20. Strauss O. The retinal pigment epithelium in visual function. Physiol Rev 2005; 85:845-81. [PMID: 15987797].

21. Campochiaro PA, Hackett SF, Conway BP. Retinoic acid promotes density-dependent growth arrest in human retinal pigment epithelial cells. Invest Ophthalmol Vis Sci 1991; 32:65-72. [PMID: 1846132].

22. Grisanti S, Guidry C. Transdifferentiation of retinal pigment epithelial cells from epithelial to mesenchymal phenotype. Invest Ophthalmol Vis Sci 1995; 36:391-405. [PMID: 7531185].

23. Anderson DH, Stern WH, Fisher SK, Erickson PA, Borgula GA. The onset of pigment epithelial proliferation after retinal detachment. Invest Ophthalmol Vis Sci 1981; 21:10-6. [PMID: 7251293].

24. Saika S, Kono-Saika S, Tanaka T, Yamanaka O, Ohnishi Y, Sato M, Muragaki Y, Ooshima A, Yoo J, Flanders KC, Roberts AB. Smad3 is required for dedifferentiation of retinal pigment epithelium following retinal detachment in mice. Lab Invest 2004; 84:1245-58. [PMID: 15273699].

25. Leontieva OV, Demidenko ZN, Blagosklonny MV. Contact inhibition and high cell density deactivate the mammalian target of rapamycin pathway, thus suppressing the senescence program. Proc Natl Acad Sci USA 2014; 111:8832-7. [PMID: 24889617].

26. Defoe DM, Levine EM. Expression of the cyclin-dependent kinase inhibitor p27Kip1 by developing retinal pigment epithelium. Gene Expr Patterns 2003; 3:615-9. [PMID: 12971995].

27. Nambu H, Yuge K, Nakajima M, Shikata N, Takahashi K, Miki H, Uyama M, Tsubura A. Morphologic characteristics of N-methyl-N-nitrosourea-induced retinal degeneration in C57BL mice. Pathol Int 1997; 47:377-83. [PMID: 9211525].

28. Fujieda H, Sasaki H. Expression of brain-derived neurotrophic factor in cholinergic and dopaminergic amacrine cells in the rat retina and the effects of constant light rearing. Exp Eye Res 2008; 86:335-43. [PMID: 18093585].

29. Poche RA, Furuta Y, Chaboissier MC, Schedl A, Behringer RR. Sox9 is expressed in mouse multipotent retinal progenitor cells and functions in Muller glial cell development. J Comp Neurol 2008; 510:237-50. [PMID: 18626943].

30. Hasson T, Heintzelman MB, Santos-Sacchi J, Corey DP, Mooseker MS. Expression in cochlea and retina of myosin VIIa, the gene product defective in Usher syndrome type 1B. Proc Natl Acad Sci USA S 1995; 92:9815-9. [PMID: 7568224].

31. el-Amraoui A, Sahly I, Picaud S, Sahel J, Abitbol M, Petit C. Human Usher 1B/mouse shaker-1: the retinal phenotype discrepancy explained by the presence/absence of myosin VIIA in the photoreceptor cells. Hum Mol Genet 1996; 5:1171-8. [PMID: 8842737].

32. Kevany BM, Palczewski K. Phagocytosis of retinal rod and cone photoreceptors. Physiology (Bethesda) 2010; 25:8-15. [PMID: 20134024].

33. Nakajima M, Nambu H, Shikata N, Senzaki H, Miki H, Tsubura A. Pigmentary degeneration induced by N-methyl-N-nitrosourea and the fate of pigment epithelial cells in the rat retina. Pathol Int 1996; 46:874-82. [PMID: 8970197].

34. Sung CH, Tai AW. Rhodopsin trafficking and its role in retinal dystrophies. Int Rev Cytol 2000; 195:215-67. [PMID: 10603577].

35. Santos AM, Martin-Oliva D, Ferrer-Martin RM, Tassi M, Calvente R, Sierra A, Carrasco MC, Marin-Teva JL, Navascues J, Cuadros MA. Microglial response to light-induced photoreceptor degeneration in the mouse retina. J Comp Neurol 2010; 518:477-92. [PMID: 20020538].

36. Hisatomi T, Sakamoto T, Sonoda KH, Tsutsumi C, Qiao H, Enaida H, Yamanaka I, Kubota T, Ishibashi T, Kura S, Susin SA, Kroemer G. Clearance of apoptotic photoreceptors: elimination of apoptotic debris into the subretinal space and macrophage-mediated phagocytosis via phosphatidylserine receptor and integrin alphavbeta3. Am J Pathol 2003; 162:1869-79. [PMID: 12759244].

37. Joly S, Francke M, Ulbricht E, Beck S, Seeliger M, Hirrlinger P, Hirrlinger J, Lang KS, Zinkernagel M, Odermatt B, Samardzija M, Reichenbach A, Grimm C, Reme CE. Cooperative phagocytes: resident microglia and bone marrow immigrants remove dead photoreceptors in retinal lesions. Am J Pathol 2009; 174:2310-23. [PMID: 19435787].

38. Imai Y, Ibata I, Ito D, Ohsawa K, Kohsaka S. A novel gene iba1 in the major histocompatibility complex class III region encoding an EF hand protein expressed in a monocytic lineage. Biochem Biophys Res Commun 1996; 224:855-62. [PMID: 8713135].

39. Hickman SE, Kingery ND, Ohsumi TK, Borowsky ML, Wang LC, Means TK, El Khoury J. The microglial sensome revealed by direct RNA sequencing. Nat Neurosci 2013; 16:1896-905. [PMID: 24162652].

40. Butovsky O, Jedrychowski MP, Moore CS, Cialic R, Lanser AJ, Gabriely G, Koeglsperger T, Dake B, Wu PM, Doykan CE, Fanek Z, Liu L, Chen Z, Rothstein JD, Ransohoff RM, Gygi SP, Antel JP, Weiner HL. Identification of a unique

TGF-beta-dependent molecular and functional signature in microglia. Nat Neurosci 2014; 17:131-43. [PMID: 24316888].

41. Chimini G, Chavrier P. Function of Rho family proteins in actin dynamics during phagocytosis and engulfment. Nat Cell Biol 2000; 2:E191-6. [PMID: 11025683].

42. Groves E, Dart AE, Covarelli V, Caron E. Molecular mechanisms of phagocytic uptake in mammalian cells. Cell Mol Life Sci 2008; 65:1957-76. [PMID: 18322649].

43. Riento K, Ridley AJ. Rocks: multifunctional kinases in cell behaviour. Nat Rev Mol Cell Biol 2003; 4:446-56. [PMID: 12778124].

44. Vicente-Manzanares M, Ma X, Adelstein RS, Horwitz AR. Non-muscle myosin II takes centre stage in cell adhesion and migration. Nat Rev Mol Cell Biol 2009; 10:778-90. [PMID: 19851336].

45. Anderson DH, Guerin CJ, Matsumoto B, Pfeffer BA. Identification and localization of a beta-1 receptor from the integrin family in mammalian retinal pigment epithelial cells. Invest Ophthalmol Vis Sci 1990; 31:81-93. [PMID: 2137116].

46. Zhao C, Yasumura D, Li X, Matthes M, Lloyd M, Nielsen G, Ahern K, Snyder M, Bok D, Dunaief JL, LaVail MM, Vollrath D. mTOR-mediated dedifferentiation of the retinal pigment epithelium initiates photoreceptor degeneration in mice. J Clin Invest 2011; 121:369-83. [PMID: 21135502].

47. Tamiya S, Liu L, Kaplan HJ. Epithelial-mesenchymal transition and proliferation of retinal pigment epithelial cells initiated upon loss of cell-cell contact. Invest Ophthalmol Vis Sci 2010; 51:2755-63. [PMID: 20042656].

48. Lee K, Nelson CM. New insights into the regulation of epithelial-mesenchymal transition and tissue fibrosis. Int Rev Cell Mol Biol 2012; 294:171-221. [PMID: 22364874].

49. Williams CD, Rizzolo LJ. Remodeling of junctional complexes during the development of the outer blood-retinal barrier. Anat Rec 1997; 249:380-8. [PMID: 9372172].

50. Joly S, Samardzija M, Wenzel A, Thiersch M, Grimm C. Nonessential role of beta3 and beta5 integrin subunits for efficient clearance of cellular debris after light-induced photoreceptor degeneration. Invest Ophthalmol Vis Sci 2009; 50:1423-32. [PMID: 18997092].

51. Ruggiero L, Connor MP, Chen J, Langen R, Finnemann SC. Diurnal, localized exposure of phosphatidylserine by rod outer segment tips in wild-type but not Itgb5−/− or Mfge8−/− mouse retina. Proc Natl Acad Sci USA 2012; 109:8145-8. [PMID: 22566632].

52. Burstyn-Cohen T, Lew ED, Traves PG, Burrola PG, Hash JC, Lemke G. Genetic dissection of TAM receptor-ligand interaction in retinal pigment epithelial cell phagocytosis. Neuron 2012; 76:1123-32. [PMID: 23259948].

53. Cardona AE, Pioro EP, Sasse ME, Kostenko V, Cardona SM, Dijkstra IM, Huang D, Kidd G, Dombrowski S, Dutta R, Lee JC, Cook DN, Jung S, Lira SA, Littman DR, Ransohoff RM. Control of microglial neurotoxicity by the fractalkine receptor. Nat Neurosci 2006; 9:917-24. [PMID: 16732273].

54. Haynes SE, Hollopeter G, Yang G, Kurpius D, Dailey ME, Gan WB, Julius D. The P2Y12 receptor regulates microglial activation by extracellular nucleotides. Nat Neurosci 2006; 9:1512-9. [PMID: 17115040].

55. Block ML, Zecca L, Hong JS. Microglia-mediated neurotoxicity: uncovering the molecular mechanisms. Nat Rev Neurosci 2007; 8:57-69. [PMID: 17180163].

56. Strick DJ, Feng W, Vollrath D. Mertk drives myosin II redistribution during retinal pigment epithelial phagocytosis. Invest Ophthalmol Vis Sci 2009; 50:2427-35. [PMID: 19117932].

57. Kalluri R, Weinberg RA. The basics of epithelial-mesenchymal transition. J Clin Invest 2009; 119:1420-8. [PMID: 19487818].

58. Vervoorts J, Luscher B. Post-translational regulation of the tumor suppressor p27(KIP1). Cell Mol Life Sci 2008; 65:3255-64. [PMID: 18636226].

59. Lamouille S, Connolly E, Smyth JW, Akhurst RJ, Derynck R. TGF-beta-induced activation of mTOR complex 2 drives epithelial-mesenchymal transition and cell invasion. J Cell Sci 2012; 125:1259-73. [PMID: 22399812].

60. Julien S, Puig I, Caretti E, Bonaventure J, Nelles L, van Roy F, Dargemont C, de Herreros AG, Bellacosa A, Larue L. Activation of NF-kappaB by Akt upregulates Snail expression and induces epithelium mesenchyme transition. Oncogene 2007; 26:7445-56. [PMID: 17563753].

61. Wang CH, Cao GF, Jiang Q, Yao J. TNF-alpha promotes human retinal pigment epithelial (RPE) cell migration by inducing matrix metallopeptidase 9 (MMP-9) expression through activation of Akt/mTORC1 signaling. Biochem Biophys Res Commun 2012; 425:33-8. [PMID: 22820188].

62. Liu Y, Xin Y, Ye F, Wang W, Lu Q, Kaplan HJ, Dean DC. Taz-tead1 links cell-cell contact to zeb1 expression, proliferation, and dedifferentiation in retinal pigment epithelial cells. Invest Ophthalmol Vis Sci 2010; 51:3372-8. [PMID: 20207963].

63. Mazzoni F, Safa H, Finnemann SC. Understanding photoreceptor outer segment phagocytosis: use and utility of RPE cells in culture. Exp Eye Res 2014; 126:51-60. [PMID: 24780752].

64. Thiery JP, Acloque H, Huang RY, Nieto MA. Epithelial-mesenchymal transitions in development and disease. Cell 2009; 139:871-90. [PMID: 19945376].

65. Elliott MR, Ravichandran KS. Clearance of apoptotic cells: implications in health and disease. J Cell Biol 2010; 189:1059-70. [PMID: 20584912].

66. Hochreiter-Hufford A, Ravichandran KS. Clearing the dead: apoptotic cell sensing, recognition, engulfment, and digestion. Cold Spring Harb Perspect Biol 2013; 5:a008748- [PMID: 23284042].

67. Plafker SM, O'Mealey GB, Szweda LI. Mechanisms for countering oxidative stress and damage in retinal pigment epithelium. Int Rev Cell Mol Biol 2012; 298:135-77. [PMID: 22878106].

Articles are provided courtesy of Emory University and the Zhongshan Ophthalmic Center, Sun Yat-sen University, P.R. China. The print version of this article was created on 23 September 2016. This reflects all typographical corrections and errata to the article through that date. Details of any changes may be found in the online version of the article.